Understanding the Multiwavelength Observation of Geminga's Tev Halo: The Role of Anisotropic Diffusion of Particles

Ruo-Yu Liu,[1,2,*] Huirong Yan,[1,3,†] and Heshou Zhang[1,3]
[1]Deutsches Elektronen Synchrotron (DESY), Platanenallee 6, D-15738 Zeuthen, Germany
[2]School of Astronomy and Space Science, Nanjing University, Nanjing 210023, China
[3]Institut für Physik und Astronomie, Universität Potsdam, D-14476 Potsdam, Germany

(Received 29 April 2019; revised manuscript received 17 September 2019; published 26 November 2019)

In this Letter, we propose that the x-ray and the TeV observations in the vicinity of Geminga can be understood in the framework of anisotropic diffusion of injected electrons or positrons. This interpretation only requires the turbulence in the vicinity of Geminga to be sub-Alfvénic with the local mean magnetic field direction approximately aligned with our line of sight towards Geminga, without invoking extreme conditions for the environment, such as an extremely small diffusion coefficient and a weak magnetic field of submicrogauss as suggested in previous literature.

DOI: 10.1103/PhysRevLett.123.221103

Introduction.—Recent observation of the High-Altitude Water Cherenkov Observatory (HAWC) has revealed a TeV γ-ray halo around the Geminga pulsar, with a spatial extension of $\gtrsim$30 pc [1]. The TeV emission is believed to arise from cosmic-ray electrons and positrons (hereafter, we do not distinguish positrons from electrons unless specified) injected from the pulsar wind nebula, via inverse-Compton (IC) scattering off cosmic microwave background photons. The detection of such a diffuse TeV emission has been interpreted as the presence of a slow diffusion zone around the pulsar [1–4] in the framework of 1D isotropic diffusion. Under the same framework, Ref. [5] studied the x-ray observation by *XMM-Newton* and *Chandra* in the vicinity of Geminga and an upper limit of 5×10^{-15} erg cm^{-2} s^{-1} in 0.7–1.3 keV has been obtained for a region within 600″ around the pulsar. This translates to an upper limit for the magnetic field strength in the TeV halo, i.e., $\leq 0.8\ \mu$G, which is significantly weaker than the typical interstellar medium (ISM) magnetic field. Furthermore, the combination of a small diffusion coefficient and a weak magnetic field would imply the saturation of the turbulence ($\delta B_g/B \simeq 1$ where δB_g is the fluctuation amplitude of magnetic field at the gyroscale of particles and B is the mean magnetic field) and the Bohm limit of diffusion, which is, however, very difficult to achieve. For interstellar turbulence, the energy injection scale is $\sim$100 pc and much larger than the gyroscale of the TeV-emitting electrons, where the resonant scattering happens. It is unlikely that $\delta B_g/B$ approaches to unity. A plausible scenario is the small-scale waves generated by instabilities. The electron flux at 100 TeV is, nonetheless, too small to generate strong enough streaming instability to overcome Landau damping [6] as well as damping by the background turbulence [7–10].

The magnetic field in ISM generally has a mean direction within one coherent length, which is typically $\sim$50–100 pc [11–13] and comparable to the size of the TeV halo. 1D particle diffusion actually cannot hold in this scenario, since particles diffuse faster along the mean magnetic field than they diffuse perpendicular to the mean magnetic field in the case of sub-Alfvénic turbulence [14–17]. Because of the anisotropy of turbulence in this case, the perpendicular diffusion coefficient is given by $D_\perp = D_\parallel M_A^4$ [14,18], where $D_\parallel$ is the diffusion coefficient parallel to the magnetic field, $M_A \equiv \delta B_{\rm inj}/B$ is the Alfvénic Mach number, which is not far from unity for ISM (i.e., $M_A > 0.1$), and $\delta B_{\rm inj}$ is the magnetic perturbation at the injection scale of magnetohydrodynamic turbulence or coherence length of magnetic field. Also, the synchrotron radiation intensity becomes anisotropic. Electrons that move along the magnetic field will radiate much less efficiently than those that move perpendicular to the magnetic field. Therefore, if the mean magnetic field in the vicinity of Geminga has a small inclination toward our line of sight (LOS), the observed synchrotron radiation flux would be much reduced compared to that with the assumption of an isotropic magnetic field, while the diffusion perpendicular to the LOS is slow as suggested by the TeV observation. Besides, the small inclination is also beneficial to reproduce the isotropic morphology of Geminga's TeV halo [17].

In this Letter, we show that both x-ray and TeV observations can be explained with typical conditions for ISM, such as the magnetic field, the diffusion coefficient, and the field perturbation level, by considering anisotropic particle diffusion which is a natural outcome in the presence of sub-Alfvénic turbulence. We will see that the viewing angle plays an important role in determining the observation signals.

 © 2019 American Physical Society

Method.—The temporal evolution of particle number density in space and energy space N is governed by the transport equation

$$\frac{\partial N}{\partial t} = \nabla \cdot (\boldsymbol{\mathcal{D}} \cdot \nabla N) - \frac{\partial}{\partial E_e}(\dot{E}_e N) + Q, \tag{1}$$

where $\dot{E}_e$ is the cooling rate of electrons due to synchrotron radiation in ISM magnetic field which is assumed to be $B = 3$ μG in this work, and IC radiation in the interstellar radiation field with considering the Klein-Nishina effect. Following [1], in addition to cosmic microwave background, we also consider an infrared photon field (with temperature 20 K and energy density 0.3 eV cm^{-3}), and an optical photon field (with temperature 5000 K and energy density 0.3 eV cm^{-3}). Q is the source term depicting the electron injection from the pulsar. $\boldsymbol{\mathcal{D}}$ is the diffusion tensor. For simplicity, we solve the equation in the cylinder coordinate, defining the z axis to be the direction of the mean magnetic field and the pulsar location to be the origin. By further assuming the system to be symmetric with respect to the z axis (i.e., $\partial/\partial\theta = 0$), we can write the transport equation into

$$\frac{\partial N}{\partial t} = \frac{1}{r}\frac{\partial}{\partial r}\left(rD_{rr}\frac{\partial N}{\partial r}\right) + D_{zz}\frac{\partial^2 N}{\partial z^2} - \frac{\partial}{\partial E_e}(\dot{E}_e N) + Q(E_e)S(t)\delta(r)\delta(z), \tag{2}$$

where the diffusion coefficient parallel to the mean magnetic field and perpendicular to it can be set, respectively, by

$$D_{zz} = D_{\parallel} = D_0(E_e/1\ \mathrm{GeV})^q, \tag{3}$$

$$D_{rr} = D_{\perp} = D_{zz}M_A^4. \tag{4}$$

Here, we neglect the drift effect which would cause asymmetric diffusion, and take $D_{\parallel}$ to be the typical ISM diffusion coefficient throughout the work which is $D_0 = 3.8 \times 10^{28}$ cm^{-2} s^{-1} and $q = 1/3$ [19]. Based on our motivation in this study, we will only look into the case with $M_A = 0.1$, 0.2, 0.3 respectively, since a larger M_A would result in a less anisotropic magnetic field topology. The rightmost term in Eq. (2) consists of three parts: the Dirac functions $\delta(r)$ and $\delta(z)$ specify the injection location, $Q(E_e, t)$ represents the injection spectrum of electron, and $S(t)$ shows the temporal behavior of the injection rate. More specifically, we assume the injection spectrum of electron to follow a power-law distribution $Q(E_e) = N_0 E_e^{-p} e^{E_e/E_{\max}}$, starting from 1 GeV. Here, N_0 is the normalization constant, p is the spectral index, and $E_{\max}$ is the high-energy cutoff energy in the spectrum. Reference [4] reported a null detection of the diffuse multi-GeV emission from the vicinity of Geminga by *Fermi* large-area telescope, suggesting a hard injection spectrum of electron from the pulsar wind nebula. We fix the value of p to be 1.6 in this work, noting that the value of p is actually not important to the predicted x-ray flux as long as the TeV observation is reproduced. $E_{\max}$ is assumed to be 200 TeV to produce a proper spectral shape measured by HAWC under the hard injection spectrum. Assuming the pulsar to be a pure dipole radiator with a braking index of 3, we have $S(t) = (1 + t/\tau)^{-2}$ with $\tau = 12$ kyr being the spin-down timescale of the pulsar. The value of N_0 is then determined by $\int\int S(t)Q(E_e)dE_e dt = W_e$, i.e., the total injected energy in cosmic-ray electrons. The evolution of the differential electron density $N(E_e, r, z, t)$ is solved by a finite difference method (see Supplemental Material [20] for details).

Next, we calculate the emissivity of electrons in the Cartesian coordinate system. Again, we put the pulsar at the origin ($x_P = 0$, $y_P = 0$, $z_P = 0$) and define the direction of the mean magnetic field as the z axis. We define the x axis so that the line connecting the pulsar and the observer, i.e., $\overline{\mathrm{PO}}$, is in the xz plane (see Fig. 1 for a sketch). Then, we envisage a random point E in the space and denote the distance between the point to the observer (i.e., the length of $\overline{\mathrm{EO}}$) by l, and denote the angle between the line $\overline{\mathrm{EO}}$ and the line $\overline{\mathrm{PO}}$ by θ. Now let us further consider a circle perpendicular to both the xz plane and the line $\overline{\mathrm{PO}}$, with its center, denoted by C, attaching to the line $\overline{\mathrm{PO}}$ and with the point E on the ring. The two intersection points of the circle and the xz plane are called point A and B, respectively, and we call the angle between the line $\overline{\mathrm{AC}}$ and the line $\overline{\mathrm{CE}}$ angle ζ. The coordinates of point E can then be given by

$$x_E = (d_{\mathrm{gem}} - l\cos\theta)\sin\phi - l\sin\theta\cos\zeta\cos\phi, \tag{5}$$

$$y_E = l\sin\theta\sin\zeta, \tag{6}$$

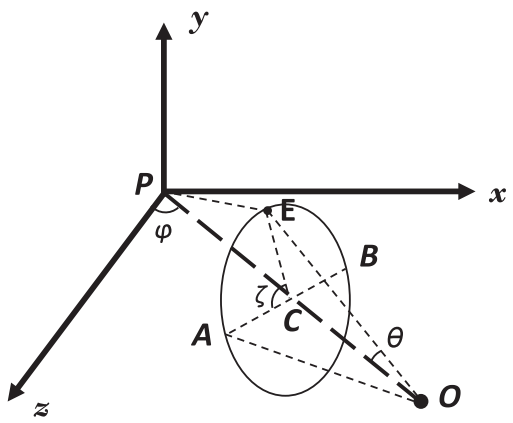

FIG. 1. Sketch figure for the geometry. See text for more details.

$$z_E = (d_{\rm gem} - l\cos\theta)\cos\phi + l\sin\theta\cos\zeta\sin\phi. \quad (7)$$

The electron density at an arbitrary point E can be found by interpolation given z_E and $r_E = \sqrt{x_E^2 + y_E^2}$, based on the obtained electron density distribution $N(E, z, r)$. The number of electron in the element volume in the neighborhood of point E can then be given by

$$dN(E, z, r) = N(E, z, r)(l\sin\theta d\zeta l d\theta dl), \quad (8)$$

where the quantity in the bracket represents the element volume around point E. Note that, although the angular distribution of electron is still isotropic (i.e., $dN/d\Omega = N(E, z, r)/4\pi$ since the mean scattering time of an electron $\sim D/c^2$ is much shorter than the cooling timescale in the energy range of interest in this work), the synchrotron radiation is anisotropic given a mean orientation of magnetic field considered in this work. Because of the relativistic beaming effect, we can only receive the radiation of electrons moving towards us and the radiation power highly depends on the pitch angle α with respect to the local magnetic field. The latter one is determined by the viewing angle ϕ and the position of the point E. If there is no magnetic field perturbation, the pitch angle can be given by $\cos\alpha_0 \equiv \vec{\rm EO}\cdot\vec{u}_z/\bar{\rm EO} = (z_O - z_E)/l = \cos\theta\cos\phi - \sin\theta\sin\phi\cos\zeta$, where $\vec{u}_z$ is the unit vector along z axis. In the presence of perturbation, the local magnetic field direction will deviate from the z axis by an angle δ. The average cosine of the pitch angle then becomes $\cos\alpha = \cos\alpha_0\cos\delta$. The distribution of $\cos^2\delta$, i.e., $f(\cos^2\delta)$, where $\int f(\cos^2\delta)d\cos^2\delta = 1$, is obtained from magnetohydrodynamic simulations for different M_A [20]. The average value of $\cos^2\delta$ is close to unity. The flux of synchrotron radiation by electrons in the element volume in the neighborhood of point E can then be given by

$$dF_{\rm syn}(\epsilon) = \int \mathcal{F}_{\rm syn}\{dN(E, z, r), B\sin\alpha\} \times f(\cos^2\delta)d\cos^2\delta/4\pi l^2. \quad (9)$$

The IC radiation is isotropic and flux can be given by

$$dF_{\rm IC}(\epsilon) = \mathcal{F}_{\rm IC}\{dN(E, z, r), n_{\rm ph}\}/4\pi l^2, \quad (10)$$

where $n_{\rm ph}$ is the differential density of the background photon field.

For observers at Earth, radiation of any electrons in LOS adds up and is projected onto the celestial sphere. The intensity at any given direction depicted by θ and ζ can then be found by $I(\epsilon, \theta, \zeta) = \int dF/\sin\theta d\theta d\zeta$. More specifically, the intensity of synchrotron radiation and the intensity of IC radiation can be given by

$$I_{\rm syn}(\epsilon, \theta, \zeta) = \frac{1}{4\pi}\int_{\cos^2\delta}\int_{l_{\rm min}}^{l_{\rm max}} \mathcal{F}_{\rm syn}\{N(E, z, r), B_0\sin\alpha\} \times f(\cos^2\delta)d\cos^2\delta dl \quad (11)$$

and

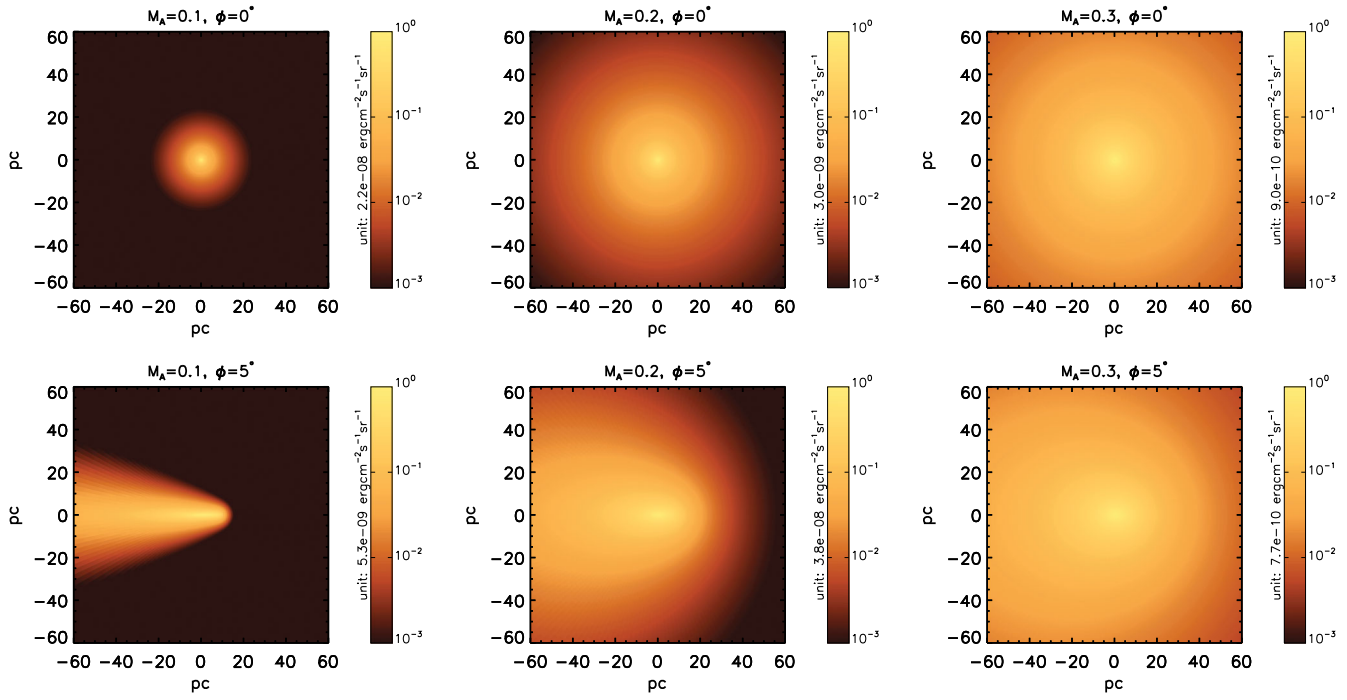

FIG. 2. Predicted 8–40 TeV SBP with different Alfvénic Mach number $M_A = 0.1$, 0.2, 0.3 and different viewing angle $\phi = 0°$, 5°.

$$I_{\rm IC}(\epsilon,\theta,\zeta)=\frac{1}{4\pi}\int_{l_{\rm min}}^{l_{\rm max}}\mathcal{F}_{\rm IC}\{N(E,z,r),n_{\rm ph}\}dl, \quad (12)$$

respectively, where $n_{\rm ph}$ is the photon number density of the background radiation. The total flux within certain angle θ_0 from the pulsar can be obtained by $F(\epsilon,\theta<\theta_0)=\int_0^{\theta_0}\int_0^{2\pi}I(\epsilon,\theta,\zeta)\sin\theta d\theta d\zeta$, where $I=I_{\rm syn}+I_{\rm IC}$.

Result.—We first show the predicted 8–40 TeV γ-ray morphology for different Alfvénic Mach number M_A and different viewing angle ϕ in Fig. 2. The Geminga pulsar is located at the center of each panel or the coordinate (0,0). The horizontal axis is parallel to the line $\overline{\rm AB}$ while the vertical axis is parallel to y axis in Fig. 1. The projected distance is calculated based on a nominal distance of 250 pc for Geminga. We can see that the morphology is too compact in the case of $\phi=0°$, $M_A=0.1$. This is because the perpendicular diffusion coefficient is only $D_\perp=3.8\times10^{24}(E_e/1\ {\rm GeV})^{1/3}\ {\rm cm^{-2}\,s^{-1}}$ for $M_A=0.1$, and the perpendicular diffusion distance is correspondingly only $\sim$5 pc within the TeV-emitting electron's cooling timescale which is $t_c\lesssim10^{12}$ s. For a viewing angle of $\phi=0°$, such a perpendicular diffusion length is translated to only $\sim1°$ extension in the celestial sphere. The morphology is highly anisotropic in the case of $\phi=5°$, $M_A=0.1$ which is obviously inconsistent with the observation. This is because the LOS towards the left side of the pulsar (e.g., direction of $\overline{\rm OA}$) passes through more electrons than the LOS towards the right side of the pulsar (e.g., direction of $\overline{\rm OB}$). On the other hand, in both of the two cases with $M_A=0.3$, the morphology does not show a sufficient gradient as that observed by HAWC. We therefore focus on the cases of $\phi=0°$ and $\phi=5°$ with $M_A=0.2$ below. A larger ϕ would result in a more anisotropic morphology and a higher x-ray flux so we do not consider it here.

We integrate the TeV emission and x-ray emission over a circular region with a radius of 10° and 600″ centered at Geminga, respectively, to compare with predicted fluxers with HAWC's observation and *XMM-Newton* upper limit. In the calculation, we adjust the value of parameter W_e to normalize the predicted TeV flux to the measured one. As we can see from Fig. 3, the predicted x-ray fluxes are lower than the upper limit of *XMM-Newton* in both two cases. The predicted surface brightness profile (SBP) in 8–40 TeV is in good agreement with the observation for $\phi=0°$. For $\phi=5°$, the predicted SBP is a little flatter than the observation. The reduced Chi-square test returns $\chi^2/{\rm dof}=1.73$ with ${\rm dof}=14$ being the degrees of freedom in the fitting. It corresponds to a p value of 0.044, implying the fitting is marginally consistent with the data at 2σ level. We therefore conclude that there should be a magnetic field alignment $\lesssim5°$ with our LOS to explain the observation for $M_A\simeq0.2$. The small inclination between the mean magnetic field and LOS is consistent with the synchrotron polarization measurement by [27] on the region of $\sim1°$

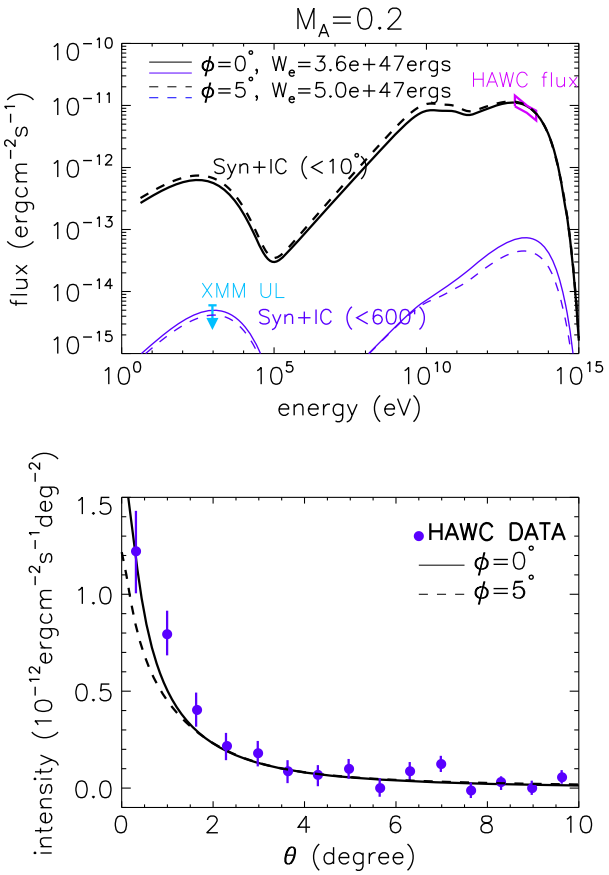

FIG. 3. Results with $\phi=0°$ and $\phi=5°$ for $M_A=0.2$. Upper: the predicted multiwavelength flux from a region within 10° from Geminga (black curves) and from a region within 600″ from Geminga (blue curves). Solid curves represent the result of $\phi=0°$ while dashed curves represent the result of $\phi=5°$. The magenta bow tie and the cyan arrow represent the flux measured by HAWC and the upper limit from *XMM-Newton* respectively. Lower: the predicted 1D (ζ averaged) SBP in 8–40 TeV in comparison with the measured one by HAWC, which is shown as blue circles.

around Geminga showing very small plane-of-sky magnetic field component. Our model can be tested in the future after many such TeV halos being detected with well determined morphologies, since it would expect (in a flux-limited sample) to observe a large number of elongated systems (B not aligned along LOS) and a minority of roughly spherical ones (B aligned along LOS) provided that M_A being significantly smaller than unity. For a larger M_A, the particle diffusion becomes more isotropic and consequently the morphology of the TeV halo would be less dependent on ϕ.

Last, we note that given the distance from Geminga to Earth being 250 pc, the intervening ISM is expected to contain two or three coherent magnetic fields. The mean magnetic field is unlikely always aligned with our LOS between Geminga and Earth. The pitch angle between the electron moving towards us and the mean field is supposed to be larger outside the TeV halo. The potential increase of

synchrotron radiation flux is, however, limited [28]. Another related issue is the contribution of Geminga to the positron excess measured in many experiments above 10 GeV [29–31]. There is a debate on the contribution of Geminga to the positron excess in the framework of inefficient (isotropic) diffusion of particles [2–4,32–34]. In the global frame from Geminga to Earth, the injected positrons from Geminga are likely to diffuse fast with the typical ISM diffusion coefficient so that the resulting positron flux at Earth can be enhanced compared to the isotropic diffusion scenario, whereas the exact flux will depend on properties of turbulence between Earth and Geminga.

*ryliu@nju.edu.cn
†huirong.yan@desy.de

[1] A. U. Abeysekara, A. Albert, R. Alfaro, C. Alvarez, J. D. Álvarez *et al.*, Science **358**, 911 (2017).
[2] K. Fang, X.-J. Bi, P.-F. Yin, and Q. Yuan, Astrophys. J. **863**, 30 (2018).
[3] S. Profumo, J. Reynoso-Cordova, N. Kaaz, and M. Silverman, Phys. Rev. D **97**, 123008 (2018).
[4] S.-Q. Xi, R.-Y. Liu, Z.-Q. Huang, K. Fang, H. Yan, and X.-Y. Wang, Astrophys. J. **878**, 104 (2019).
[5] R.-Y. Liu, C. Ge, X.-N. Sun, and X.-Y. Wang, Astrophys. J. **875**, 149 (2019).
[6] R. Kulsrud and W. P. Pearce, Astrophys. J. **156**, 445 (1969).
[7] A. J. Farmer and P. Goldreich, Astrophys. J. **604**, 671 (2004).
[8] H. Yan and A. Lazarian, Astrophys. J. **614**, 757 (2004).
[9] A. Lazarian, Astrophys. J. **833**, 131 (2016).
[10] K. Fang, X.-J. Bi, and P.-F. Yin, Mon. Not. R. Astron. Soc. **488**, 4074 (2019).
[11] J. Cho and D. Ryu, Astrophys. J. Lett. **705**, L90 (2009).
[12] A. Chepurnov and A. Lazarian, Astrophys. J. **710**, 853 (2010).
[13] M. C. Beck, A. M. Beck, R. Beck, K. Dolag, A. W. Strong, and P. Nielaba, J. Cosmol. Astropart. Phys. 05 (2016) 056.
[14] H. Yan and A. Lazarian, Astrophys. J. **673**, 942 (2008).
[15] G. Giacinti and G. Sigl, Phys. Rev. Lett. **109**, 071101 (2012).
[16] L. Nava and S. Gabici, Mon. Not. R. Astron. Soc. **429**, 1643 (2013).
[17] R. López-Coto and G. Giacinti, Mon. Not. R. Astron. Soc. **479**, 4526 (2018).
[18] S. Xu and H. Yan, Astrophys. J. **779**, 140 (2013).
[19] R. Trotta, G. Jóhannesson, I. V. Moskalenko, T. A. Porter, R. Ruiz de Austri, and A. W. Strong, Astrophys. J. **729**, 106 (2011).
[20] See Supplemental Material at http://link.aps.org/supplemental/10.1103/PhysRevLett.123.221103, which includes Refs. [21–26], for a detailed treatment.
[21] K. D. Makwana and H. Yan, arXiv:1907.01853.
[22] A. Brandenburg and W. Dobler, Comput. Phys. Commun. **147**, 471 (2002).
[23] A. Brandenburg and W. Dobler, *Pencil: Finite-Difference Code for Compressible Hydrodynamic Flows* (Astrophysics Source Code Library, 2010).
[24] A. Mignone, G. Bodo, S. Massaglia, T. Matsakos, O. Tesileanu, C. Zanni, and A. Ferrari, Astrophys. J. Suppl. Ser. **170**, 228 (2007).
[25] A. Mignone, C. Zanni, P. Tzeferacos, B. van Straalen, P. Colella, and G. Bodo, Astrophys. J. Suppl. Ser. **198**, 7 (2012).
[26] A. Lazarian and D. Pogosyan, Astrophys. J. **747**, 5 (2012).
[27] X. Y. Gao, W. Reich, J. L. Han, X. H. Sun, R. Wielebinski, W. B. Shi, L. Xiao, P. Reich, E. Fürst, M. Z. Chen *et al.*, Astron. Astrophys. **515**, A64 (2010).
[28] Even in the extreme case of a mean magnetic field perpendicular to LOS (or 90° pitch angle) outside the TeV halo, the synchrotron flux can still be consistent with the upper limit by employing a slightly weaker magnetic field of 2 μG for the intervening medium.
[29] O. Adriani, G. C. Barbarino, G. A. Bazilevskaya, R. Bellotti, M. Boezio, E. A. Bogomolov, L. Bonechi, M. Bongi, V. Bonvicini, S. Bottai *et al.*, Nature (London) **458**, 607 (2009).
[30] M. Ackermann, M. Ajello, A. Allafort, W. B. Atwood, L. Baldini, G. Barbiellini, D. Bastieri, K. Bechtol, R. Bellazzini, B. Berenji *et al.*, Phys. Rev. Lett. **108**, 011103 (2012).
[31] M. Aguilar, D. Aisa, A. Alvino, G. Ambrosi, K. Andeen, L. Arruda, N. Attig, P. Azzarello, A. Bachlechner, F. Barao *et al.*, Phys. Rev. Lett. **113**, 121102 (2014).
[32] D. Hooper, I. Cholis, T. Linden, and K. Fang, Phys. Rev. D **96**, 103013 (2017).
[33] X. Tang and T. Piran, Mon. Not. R. Astron. Soc. **484**, 3491 (2019).
[34] M. Di Mauro, S. Manconi, and F. Donato, arXiv:1903.05647.